High resolution infrared emission spectra of AlH and AlD

J. B. White, M. Dulick, and P. F. Bernath
Centre for Molecular Beams and Laser Chemistry, Department of Chemistry, University of Waterloo, Waterloo, Ontario N2L 3G1, Canada

High resolution infrared emission spectra of aluminum monohydride and monodeuteride have been recorded. Gaseous AlH and AlD were generated by reacting molten aluminum metal with hydrogen and deuterium gas. Approximately 265 AlH lines with $v=1\to0$ to $v=5\to4$ and 470 AlD lines with $v=1\to0$ to $v=7\to6$ are reported. Dunham Y_{ij} constants were obtained by fitting the data of each isotopomer separately to the Dunham energy level expression while mass-reduced Dunham U_{ij} constants were obtained from a combined fit of all isotopomer data. A second set of Dunham U_{ij} constants was obtained from a fit where U_{ij}'s with $j<2$ were treated as adjustable parameters and all remaining U_{ij}'s fixed to values that satisfy the constraints imposed by the Dunham model. Finally, an effective Born–Oppenheimer potential was determined by fitting all the data directly to the eigenvalues of the radial Schrödinger equation containing a parametrized potential function.

I. INTRODUCTION

AlH has been receiving a great deal of attention in recent years. For instance, AlH is a potential candidate for an advanced chemical rocket propellant that involves trapping metal hydride molecules inside cryogenic matrices.[1] AlH continues to be of interest to astronomers since its presence has been detected in the stellar atmospheres of M-type and S-type stars[2-4] as well as in sunspots.[5]

The electronic structure of AlH has been the subject of intense scrutiny by theoreticians over the last several decades. Starting in 1966 with a calculation on the Rydberg states[6] there is a voluminous literature on the properties of the ground and excited electronic states obtained by *ab initio* calculations.[7-20] Of noteworthy importance are the most recent complete active space self-consistent field (CASSCF) calculations reported by Matos, Malmqvist, and Roos[15] as well as the CASSCF+CI calculation by Bauschlicher and Langhoff.[19] On the basis of the theoretically derived dipole moment function,[10] Tipping *et al.*[17] predict very strong vibration-rotation transitions in the ground electronic state with the Einstein A coefficient estimated to be 208 s^{-1} for the 1–0 band. AlH is very similar[17] to CO in the sense that AlH possesses a small dipole moment, $\mu_e = -0.10$ D, but a large dipole moment derivative, $d\mu/dr = -3.8$ D/Å.[10]

On the experimental side, an extensive number of classical spectroscopic studies were devoted to the analyses of both the AlH and AlD electronic spectra.[21-32] Both singlet–singlet and triplet–triplet electronic transitions are known. Perhaps the best and most extensive analysis of an electronic transition to date is the reported analysis of $A\,^1\Pi$-$X\,^1\Sigma^+$ by Zeeman and Ritter.[28] In a more recent development, AlH and AlD have also been the subjects of study by pulsed laser spectroscopy.[33-36] The lifetime of the $A\,^1\Pi$ state was measured through fluorescence decay[33] and the $b\,^3\Sigma^-$-$X\,^1\Sigma^+$ intercombination electronic transition was recorded and analyzed by Zhu, Shehadeh, and Grant.[36]

Vibrational-rotational diode laser spectra were re-

corded for AlD by Urban and Jones[37] and for AlH by Yamada and Hirota.[38] Both studies measured only a relatively small number of lines involving the fundamental and several hot bands with a nominal accuracy of ±0.001 cm^{-1}. The first overtone band of AlH was recorded in emission by Deutsch, Neil, and Ramsay[39] with a Fourier transform spectrometer. Although their data set is quite extensive, the quality of the data are questionable in light of the fact that the lines suffer from the effects of pressure broadening.

We report here on extensive emission spectra of the fundamental and several hot bands of AlH and AlD with rotational lines measured to a precision of ±0.0002 cm^{-1}.

II. EXPERIMENT

High resolution emission spectra of AlH and AlD were recorded with a Bruker IFS 120 HR Fourier transform spectrometer at the University of Waterloo. Both AlH and AlD were produced in the gas phase through a chemical reaction involving 30 g of molten aluminum with either 20 Torr of hydrogen or deuterium gas over an operating temperature range of 1100 °C–1550 °C (Al vapor pressure ~ 1 Torr at 1545 °C). The cell design consisted of a 1.2 m long mullite ($3Al_2O_3 \cdot 2SiO_2$) tube with the central portion of the tube placed inside of a CM Rapid Temp Furnace. The mullite tube was protected from the corrosive molten aluminum by a carbon liner tube. In order to prevent the mullite tube from cracking, the cell was brought up gradually to operating temperature by setting the heating rate at 200 °C/h.

Impurities from the system were removed prior to the actual experiment by pumping on the heated cell up to a maximum temperature of 1000 °C. Above this temperature, the pumping port was sealed and 5 Torr of argon buffer gas was added to prevent deposition of material on the cell windows, followed by the addition of 20 Torr of H_2 or D_2 at 1100 °C. Weak emission, attributed to AlH (or AlD), was first seen at 1460 °C. The molecular emission

FIG. 1. The infrared emission spectrum of AlH.

FIG. 3. Expanded view of the R-branch bandhead of the AlH $v=1 \rightarrow 0$ band.
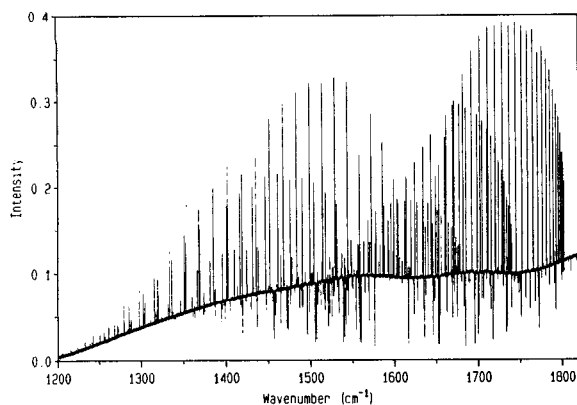
increased in intensity with increasing temperature until 1550 °C, at which point high resolution spectra were recorded.

The high resolution spectrum of AlH was recorded at a resolution of 0.005 cm^{-1} over the range 1150–2200 cm^{-1} with a HgCdTe detector, CaF$_2$ beamsplitter, and CaF$_2$ cell windows. The lower wave-number limit of 1150 cm^{-1} was set by the transmission of the CaF$_2$ beamsplitter while the upper limit of 2200 cm^{-1} was set by a red pass optical filter. To record the spectrum of AlD at a resolution of 0.006 cm^{-1} over the range 850–1672 cm^{-1} required switching to a KBr beamsplitter and KBr windows. Once again a red pass optical filter was selected to set the upper wave-number limit to 1672 cm^{-1} while the 850 cm^{-1} lower limit was determined by HgCdTe detector response. The final AlH and AlD spectra consisted of 64 and 39 coadded scans, respectively. An overall view of the AlH and AlD spectra are displayed in Figs. 1 and 2.

III. RESULTS AND DISCUSSION

Assignment of AlH and AlD bands was facilitated by an interactive color Loomis–Wood program. Rotational lines were measured using the computer program PC-DECOMP written by Brault. Line centers are determined by
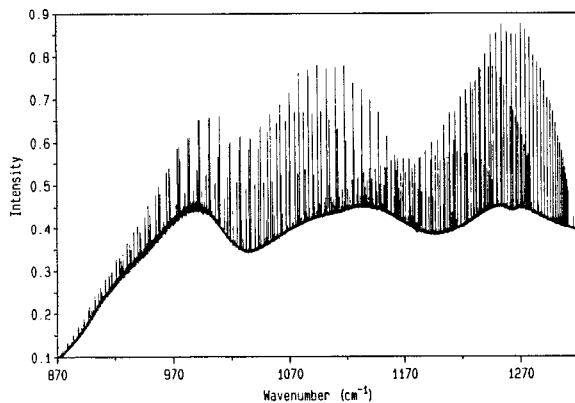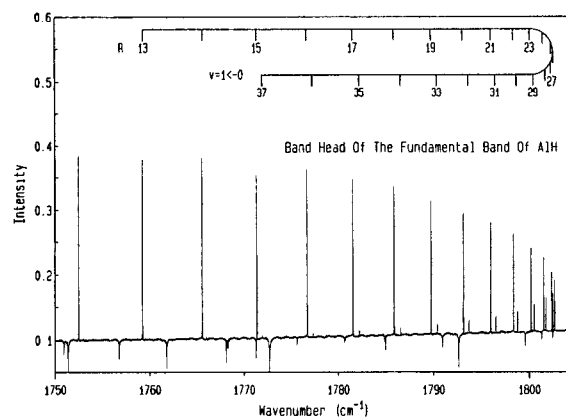
fitting measured line profiles to Voigt line shape functions. Water lines, which are usually present in our spectra as an impurity, were used in the absolute calibration of the AlD spectrum.[40] The lines in the AlH spectrum were then calibrated with respect to AlD lines since AlD was present as an impurity in the AlH spectrum. The strongest AlH and AlD lines with a signal to noise ratio of 150 were measured to a precision of ±0.0002 cm^{-1} while the weakest and blended lines were measured at a lesser precision of ±0.005 cm^{-1}. The error in the absolute calibration of the line positions is estimated to be ±0.0002 cm^{-1} but another independent measurement is necessary to verify this. The high quality of the AlH and AlD spectra are illustrated in Figs. 3 and 4 in the vicinity of the R-branch band heads of their respective $v=1 \rightarrow 0$ bands. And finally, a list of all observed AlH and AlD lines are given in Table I.

Dunham Y_{ij} constants for AlH and AlD, listed in Table II, were obtained by fitting the data set of each isotopomer to the energy level expression[41]

$$E(v,J) = \sum_{i,j} Y_{ij} \left(v + \frac{1}{2} \right)^i [J(J+1)]^j \qquad (1)$$

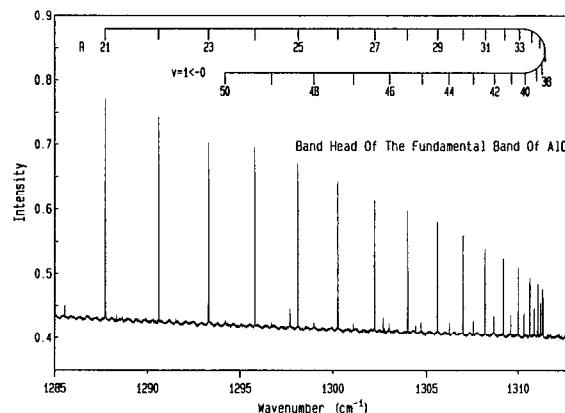FIG. 2. The infrared emission spectrum of AlD.

FIG. 4. Expanded view of the R-branch bandhead of the AlD $v=1 \rightarrow 0$ band.

TABLE I. Observed line positions of (a) AlH and (b) AlD in cm^{-1}. The observed–calculated (column labeled Δ) correspond to the constrained fit with the mass-reduced Dunham constants listed in Table III.

Line	Observed	Δ	Line	Observed	Δ	Line	Observed	Δ	Line	Observed	Δ
						(1,0) Band					
(a)											
			P(24)	1 242.826 11	19	P(23)	1 261.267 75	26	P(22)	1 279.561 77	42
P(21)	1 297.698 22	26	P(20)	1 315.667 91	17	P(19)	1 333.461 10	8	P(18)	1 351.068 13	1
P(17)	1 368.479 28	−3	P(16)	1 385.684 86	2	P(15)	1 402.674 87	−6	P(14)	1 419.439 65	−12
P(13)	1 435.969 53	−7	P(12)	1 452.254 57	−3	P(11)	1 468.284 99	−4	P(10)	1 484.051 11	−2
P(9)	1 499.543 20	1	P(8)	1 514.751 55	−1	P(7)	1 529.666 66	4	P(6)	1 544.278 91	7
P(5)	1 558.578 98	22	P(4)	1 572.557 06	6	P(3)	1 586.204 41	12	P(2)	1 599.511 59	12
P(1)	1 612.469 56	6	R(0)	1 637.302 73	12	R(1)	1 649.160 42	10	R(2)	1 660.634 21	7
R(3)	1 671.715 85	5	R(4)	1 682.397 28	6	R(5)	1 692.670 54	3	R(6)	1 702.527 99	0
R(7)	1 711.962 18	−1	R(8)	1 720.965 83	−3	R(9)	1 729.531 94	−5	R(10)	1 737.653 80	−3
R(11)	1 745.324 79	−6	R(12)	1 752.538 77	−2	R(13)	1 759.289 61	−6	R(14)	1 765.571 72	−5
R(15)	1 771.379 63	−2	R(16)	1 776.708 09	−6	R(17)	1 781.552 35	−5	R(18)	1 785.907 81	−4
R(19)	1 789.770 19	−3	R(20)	1 793.135 50	−4	R(21)	1 796.000 07	−7	R(22)	1 798.360 63	−6
R(23)	1 800.214 09	−3	R(24)	1 801.557 65	−6	R(25)	1 802.388 97	−7	R(26)	1 802.705 83	−16
R(27)	1 802.506 80	4	R(28)	1 801.789 69	−17	R(29)	1 800.553 90	−19	R(30)	1 798.798 38	−20
R(31)	1 796.522 59	−15	R(32)	1 793.726 23	−4	R(33)	1 790.408 80	−37	R(34)	1 786.572 03	31
R(35)	1 782.214 74	27	R(36)	1 777.339 04	80	R(37)	1 771.943 35	−77	R(38)	1 766.032 77	−66
R(39)	1 759.608 09	36									
						(2,1) Band					
P(22)	1 233.080 21	13	P(21)	1 250.736 63	15	P(20)	1 268.229 84	9	P(19)	1 285.550 73	30
P(18)	1 302.689 09	9	P(17)	1 319.635 94	3	P(16)	1 336.381 56	−2	P(15)	1 352.916 33	−6
P(14)	1 369.230 66	−6	P(13)	1 385.314 89	−6	P(12)	1 401.159 35	−11	P(11)	1 416.754 55	−10
P(10)	1 432.090 84	−8	P(9)	1 447.158 66	−8	P(8)	1 461.948 55	−6	P(7)	1 476.451 01	−7
P(6)	1 490.656 73	−4	P(5)	1 504.556 42	4	P(4)	1 518.140 71	1	P(3)	1 531.400 60	−1
P(2)	1 544.327 19	9	P(1)	1 556.911 26	−4	R(0)	1 581.017 84	−8	R(1)	1 592.523 32	5
R(2)	1 603.652 22	1	R(3)	1 614.396 61	1	R(4)	1 624.748 51	−2	R(5)	1 634.700 20	−3
R(6)	1 644.244 20	2	R(7)	1 653.373 15	11	R(8)	1 662.079 69	−3	R(9)	1 670.357 30	−4
R(10)	1 678.199 28	0	R(11)	1 685.599 11	−3	R(12)	1 692.550 77	−3	R(13)	1 699.048 33	−5
R(14)	1 705.086 25	−5	R(15)	1 710.659 18	−4	R(16)	1 715.762 11	2	R(17)	1 720.390 15	−1
R(18)	1 724.538 99	4	R(19)	1 728.204 29	1	R(20)	1 731.382 28	2	R(21)	1 734.069 35	5
R(22)	1 736.262 14	3	R(23)	1 737.957 73	3	R(24)	1 739.153 41	5	R(25)	1 739.848 61	189
R(26)	1 740.035 80	15	R(27)	1 739.718 37	0	R(28)	1 738.893 47	11	R(29)	1 737.559 30	−10
R(30)	1 735.715 42	−11	R(31)	1 733.359 73	−137	R(32)	1 730.496 14	43	R(33)	1 727.118 90	−33
R(34)	1 723.232 59	82	R(35)	1 718.833 58	−11	R(36)	1 713.925 34	−26	R(37)	1 708.508 31	2
						(3,2) Band					
			P(19)	1 238.852 69	28	P(18)	1 255.533 80	−9	P(17)	1 272.027 68	6
P(16)	1 288.324 19	0	P(15)	1 304.413 99	−20	P(14)	1 320.287 94	−24	P(13)	1 335.936 69	−3
P(12)	1 351.350 35	−3	P(11)	1 366.519 65	−6	P(10)	1 381.435 17	−15	P(9)	1 396.087 67	−16
P(8)	1 410.467 75	−16	P(7)	1 424.565 98	−31	P(6)	1 438.373 71	−4	P(5)	1 451.881 17	1
P(4)	1 465.079 56	10	P(3)	1 477.959 82	11	P(2)	1 490.513 00	−5	P(1)	1 502.730 74	−2
R(0)	1 526.124 93	−9	R(1)	1 537.284 80	−1	R(2)	1 548.075 36	−10	R(3)	1 558.488 70	−29
R(4)	1 568.517 63	3	R(5)	1 578.153 72	3	R(6)	1 587.389 86	−1	R(7)	1 596.218 93	−1
R(8)	1 604.633 98	6	R(9)	1 612.628 08	1	R(10)	1 620.194 82	−5	R(11)	1 627.328 06	0
R(12)	1 634.021 55	−6	R(13)	1 640.269 75	−2	R(14)	1 646.067 09	7	R(15)	1 651.408 11	−2
R(16)	1 656.288 06	−8	R(17)	1 660.702 32	−4	R(18)	1 664.646 36	−2	R(19)	1 668.116 02	−5
R(20)	1 671.107 66	8	R(21)	1 673.617 46	9	R(22)	1 675.642 32	17	R(23)	1 677.179 14	20
R(24)	1 678.225 43	40	R(25)	1 678.778 06	5	R(26)	1 678.835 82	10	R(27)	1 678.396 29	−1
R(28)	1 677.457 81	−34	R(29)	1 676.019 91	−3	R(30)	1 674.081 15	56	R(31)	1 671.640 26	99
R(32)	1 668.695 68	29	R(33)	1 665.247 65	−95	R(34)	1 661.294 74	−400	R(35)	1 656.843 80	−208
						(4,3) Band					
P(17)	1 225.573 47	67	P(16)	1 241.431 19	−104	P(15)	1 257.089 00	1	P(14)	1 272.534 11	28
P(13)	1 287.757 65	14	P(12)	1 302.750 53	−26	P(11)	1 317.504 33	−9	P(10)	1 332.009 33	14
P(9)	1 346.255 96	5	P(8)	1 360.235 63	21	P(7)	1 373.938 76	13	P(6)	1 387.356 48	−2
P(5)	1 400.479 83	−23	P(4)	1 413.300 38	−4	P(3)	1 425.808 43	−37	P(2)	1 437.996 65	13
P(1)	1 449.852 00	−299	R(0)	1 472.550 68	11	R(1)	1 483.371 52	31	R(2)	1 493.829 78	8
R(3)	1 503.918 41	22	R(4)	1 513.629 09	6	R(5)	1 522.955 21	46	R(6)	1 531.888 16	9
R(7)	1 540.422 16	24	R(8)	1 548.549 52	9	R(9)	1 556.264 05	8	R(10)	1 563.559 14	0
R(11)	1 570.428 83	8	R(12)	1 576.866 99	12	R(13)	1 582.867 88	5	R(14)	1 588.426 28	10
R(15)	1 593.537 05	30	R(16)	1 598.194 67	4	R(17)	1 602.395 23	5	R(18)	1 606.134 24	23
R(19)	1 609.407 09	8	R(20)	1 612.210 37	4	R(21)	1 614.540 59	18	R(22)	1 616.394 31	36
R(23)	1 617.767 79	−11	R(24)	1 618.659 69	18	R(25)	1 619.067 34	109	R(26)	1 618.985 39	−49
R(27)	1 618.416 56	17	R(28)	1 617.355 54	−49	R(29)	1 615.804 46	119	R(30)	1 613.756 85	3
						(5,4) Band					
P(13)	1 240.685 41	−66	P(12)	1 255.269 95	−30	P(11)	1 269.620 05	100	P(10)	1 283.722 90	−53
P(9)	1 297.574 23	−17	P(8)	1 311.163 19	18	P(7)	1 324.480 01	−32	P(6)	1 337.516 94	−57

TABLE I. (*Continued.*)

Line	Observed	Δ	Line	Observed	Δ	Line	Observed	Δ	Line	Observed	Δ
P(5)	1 350.265 09	−66	P(4)	1 362.716 90	57	P(3)	1 374.860 23	−42	P(2)	1 386.692 44	228
R(1)	1 430.692 60	−123	R(2)	1 440.815 59	−1013	R(3)	1 450.594 45	9	R(4)	1 459.991 66	−54
R(5)	1 469.011 52	−38	R(6)	1 477.646 48	19	R(7)	1 485.888 20	−21	R(8)	1 493.731 05	−44
R(9)	1 501.169 05	6	R(10)	1 508.194 16	−42	R(11)	1 514.802 34	18	R(12)	1 520.985 44	−41
R(13)	1 526.739 93	−11	R(14)	1 532.059 29	−3	R(15)	1 536.938 03	−52	R(16)	1 541.372 78	−6
R(17)	1 545.357 37	−17	R(18)	1 548.888 63	38	R(19)	1 551.961 04	19	R(20)	1 554.572 84	140
R(21)	1 556.716 43	5									

(b)

Line	Observed	Δ	Line	Observed	Δ	Line	Observed	Δ	Line	Observed	Δ
						(1,0) Band					
			P(38)	858.669 36	98	P(37)	868.537 80	17	P(36)	878.363 96	−37
P(35)	888.145 81	−15	P(34)	897.879 83	−18	P(33)	907.563 82	−13	P(32)	917.194 90	−31
P(31)	926.771 08	−17	P(30)	936.289 37	−11	P(29)	945.747 05	−26	P(28)	955.141 89	−25
P(27)	964.471 34	−2	P(26)	973.732 32	−3	P(25)	982.922 39	−10	P(24)	992.039 11	−2
P(23)	1 001.079 60	−5	P(22)	1 010.037 00	−438	P(21)	1 018.921 60	−10	P(20)	1 027.717 90	−4
P(19)	1 036.427 30	−15	P(18)	1 045.047 50	−8	P(17)	1 053.575 70	1	P(16)	1 062.009 10	−2
P(15)	1 070.345 30	6	P(14)	1 078.581 50	9	P(13)	1 086.715 00	0	P(12)	1 094.743 40	2
P(11)	1 102.664 00	4	P(10)	1 110.474 20	7	P(9)	1 118.171 30	0	P(8)	1 125.752 90	0
P(7)	1 133.216 40	1	P(6)	1 140.559 30	9	P(5)	1 147.779 00	14	P(4)	1 154.872 90	7
P(3)	1 161.838 70	4	P(2)	1 168.674 00	12	P(1)	1 175.376 20	13	R(0)	1 188.371 90	9
R(1)	1 194.660 60	−4	R(2)	1 200.807 10	8	R(3)	1 206.808 70	2	R(4)	1 212.663 40	3
R(5)	1 218.368 90	2	R(6)	1 223.923 00	−6	R(7)	1 229.323 70	−6	R(8)	1 234.568 90	0
R(9)	1 239.656 40	−3	R(10)	1 244.584 30	−5	R(11)	1 249.350 60	−9	R(12)	1 253.953 50	−4
R(13)	1 258.391 00	−2	R(14)	1 262.661 30	−3	R(15)	1 266.762 60	−9	R(16)	1 270.693 30	−7
R(17)	1 274.451 70	0	R(18)	1 278.036 00	−7	R(19)	1 281.444 80	−12	R(20)	1 284.676 70	−3
R(21)	1 287.730 00	−5	R(22)	1 290.603 40	−8	R(23)	1 293.295 60	−7	R(24)	1 295.805 30	−4
R(25)	1 298.131 20	−7	R(26)	1 300.272 20	−9	R(27)	1 302.227 20	−7	R(28)	1 303.995 20	1
R(29)	1 305.575 00	−4	R(30)	1 306.965 90	0	R(31)	1 308.166 90	0	R(32)	1 309.177 20	−2
R(33)	1 309.996 10	−4	R(34)	1 310.623 10	15	R(35)	1 311.057 70	17	R(36)	1 311.297 90	7
R(37)	1 311.344 90	6	R(38)	1 311.197 80	19	R(39)	1 310.856 10	33	R(40)	1 310.319 00	−1
R(41)	1 309.587 10	6	R(42)	1 308.659 60	−9	R(43)	1 307.537 30	50	R(44)	1 306.218 30	0
R(45)	1 304.704 40	25	R(46)	1 302.993 90	−50	R(47)	1 301.089 90	78	R(48)	1 298.988 60	14
R(49)	1 296.693 30	68	R(52)	1 288.636 70	−5						
						(2,1) Band					
P(36)	855.000 78	137	P(35)	864.595 15	41	P(34)	874.142 68	−65	P(33)	883.642 82	16
P(32)	893.090 58	35	P(31)	902.483 45	−7	P(30)	911.819 96	0	P(29)	921.097 00	−2
P(28)	930.312 08	−4	P(27)	939.462 85	16	P(26)	948.546 17	3	P(25)	957.559 82	−5
P(24)	966.501 37	9	P(23)	975.367 88	12	P(22)	984.156 75	5	P(21)	992.865 51	2
P(20)	1 001.491 50	0	P(19)	1 010.037 00	489	P(18)	1 018.484 80	9	P(17)	1 026.846 70	3
P(16)	1 035.115 40	2	P(15)	1 043.288 30	7	P(14)	1 051.362 70	9	P(13)	1 059.336 00	7
P(12)	1 067.205 70	11	P(11)	1 074.969 10	8	P(10)	1 082.623 80	15	P(9)	1 090.167 00	8
P(8)	1 097.596 40	11	P(7)	1 104.909 30	7	P(6)	1 112.103 40	15	P(5)	1 119.175 90	5
P(4)	1 126.124 60	3	P(3)	1 132.947 10	15	P(2)	1 139.640 50	−9	P(1)	1 146.203 00	−7
R(0)	1 158.925 20	5	R(1)	1 165.080 30	20	R(2)	1 171.094 60	1	R(3)	1 176.966 40	1
R(4)	1 182.693 10	−18	R(5)	1 188.273 10	2	R(6)	1 193.703 70	4	R(7)	1 198.983 00	8
R(8)	1 204.108 80	2	R(9)	1 209.079 30	6	R(10)	1 213.892 30	−2	R(11)	1 218.546 10	2
R(12)	1 223.038 60	−4	R(13)	1 227.368 10	−5	R(14)	1 231.532 80	−2	R(15)	1 235.530 90	−1
R(16)	1 239.360 70	−2	R(17)	1 243.020 60	0	R(18)	1 246.509 00	3	R(19)	1 249.824 30	2
R(20)	1 252.965 10	5	R(21)	1 255.929 90	5	R(22)	1 258.717 30	0	R(23)	1 261.326 10	2
R(24)	1 263.755 00	8	R(25)	1 266.002 70	8	R(26)	1 268.068 10	6	R(27)	1 269.950 20	13
R(28)	1 271.647 80	10	R(29)	1 273.160 10	16	R(30)	1 274.486 00	12	R(31)	1 275.624 30	−37
R(32)	1 276.575 30	−21	R(33)	1 277.338 50	82	R(34)	1 277.912 10	162	R(35)	1 278.294 80	148
R(36)	1 278.486 30	68	R(44)	1 273.118 00	31	R(45)	1 271.580 00	15	R(46)	1 269.848 80	−31
R(47)	1 267.925 80	29	R(48)	1 265.808 40	−79	R(49)	1 263.500 20	−11			
						(3,2) Band					
P(34)	850.849 60	−107	P(33)	860.169 90	106	P(32)	869.435 61	−46	P(31)	878.649 93	6
P(30)	887.807 65	−7	P(29)	896.906 87	−26	P(28)	905.945 72	17	P(27)	914.920 46	2
P(26)	923.829 33	7	P(25)	932.669 42	−2	P(24)	941.438 11	−30	P(23)	950.133 57	−4
P(22)	958.752 49	4	P(21)	967.292 35	0	P(20)	975.750 57	−16	P(19)	984.125 00	1
P(18)	992.412 51	−5	P(17)	1 000.610 80	−4	P(16)	1 008.717 40	15	P(15)	1 016.729 30	8
P(14)	1 024.644 20	3	P(13)	1 032.459 60	6	P(12)	1 040.172 80	4	P(11)	1 047.781 30	1
P(10)	1 055.282 70	10	P(9)	1 062.674 20	5	P(8)	1 069.953 50	5	P(7)	1 077.118 10	11
P(6)	1 084.165 30	−1	P(5)	1 091.093 10	17	P(4)	1 097.898 40	−4	P(3)	1 104.579 40	0
P(2)	1 111.133 50	6	P(1)	1 117.558 00	−19	R(0)	1 130.010 20	−27	R(1)	1 136.033 30	−11
R(2)	1 141.917 80	−7	R(3)	1 147.661 60	−4	R(4)	1 153.262 50	−4	R(5)	1 158.718 40	0
R(6)	1 164.027 10	−3	R(7)	1 169.186 70	5	R(8)	1 174.194 90	−3	R(9)	1 179.049 90	−7
R(10)	1 183.749 80	−2	R(11)	1 188.292 50	−8	R(12)	1 192.676 40	1	R(13)	1 196.899 40	−3

TABLE I. (*Continued.*)

Line	Observed	Δ	Line	Observed	Δ	Line	Observed	Δ	Line	Observed	Δ
$R(14)$	1 200.959 90	−3	$R(15)$	1 204.856 10	−8	$R(16)$	1 208.586 40	−9	$R(17)$	1 212.149 20	−5
$R(18)$	1 215.542 80	−10	$R(19)$	1 218.765 80	−11	$R(20)$	1 221.816 70	−11	$R(21)$	1 224.694 20	−1
$R(22)$	1 227.396 60	−13	$R(23)$	1 229.923 00	−8	$R(24)$	1 232.271 90	−12	$R(25)$	1 234.442 30	−4
$R(26)$	1 236.432 90	−3	$R(27)$	1 238.242 60	−10	$R(28)$	1 239.870 60	−4	$R(29)$	1 241.315 80	2
$R(30)$	1 242.577 20	−2	$R(31)$	1 243.654 10	−2	$R(32)$	1 244.545 70	1	$R(33)$	1 245.251 10	−9
$R(34)$	1 245.770 00	4	$R(35)$	1 246.101 30	−9	$R(36)$	1 246.244 60	−31	$R(37)$	1 246.199 90	−12
$R(38)$	1 245.966 30	1	$R(39)$	1 245.543 40	7	$R(40)$	1 244.931 10	31	$R(41)$	1 244.128 40	−2
$R(42)$	1 243.136 10	13	$R(43)$	1 241.953 90	61	$R(44)$	1 240.580 50	25	$R(45)$	1 239.017 30	52
$R(46)$	1 237.262 30	−56	$R(47)$	1 235.317 20	−133	$R(48)$	1 233.184 60	75			

(4,3) Band

Line	Observed	Δ	Line	Observed	Δ	Line	Observed	Δ	Line	Observed	Δ
$P(31)$	855.250 00	117	$P(30)$	864.226 05	−557	$P(29)$	873.155 64	−116	$P(28)$	882.021 32	−56
$P(27)$	890.824 65	28	$P(26)$	899.561 88	13	$P(25)$	908.231 96	46	$P(24)$	916.831 19	10
$P(23)$	925.357 54	−45	$P(22)$	933.809 70	5	$P(21)$	942.183 41	−12	$P(20)$	950.476 88	−19
$P(19)$	958.687 34	−39	$P(18)$	966.813 02	7	$P(17)$	974.850 32	13	$P(16)$	982.796 32	−58
$P(15)$	990.650 14	−38	$P(14)$	998.408 52	−1	$P(13)$	1 006.068 30	−8	$P(12)$	1 013.627 50	−6
$P(11)$	1 021.083 60	5	$P(10)$	1 028.433 90	6	$P(9)$	1 035.676 10	14	$P(8)$	1 042.807 40	0
$P(7)$	1 049.825 80	7	$P(6)$	1 056.728 50	2	$P(5)$	1 063.513 40	16	$P(4)$	1 070.177 70	10
$P(3)$	1 076.719 00	−18	$P(2)$	1 083.135 50	−12	$P(1)$	1 089.424 70	13	$R(0)$	1 101.611 20	36
$R(1)$	1 107.503 40	−21	$R(2)$	1 113.259 90	6	$R(3)$	1 118.877 30	−4	$R(4)$	1 124.354 00	5
$R(5)$	1 129.687 50	−5	$R(6)$	1 134.876 10	4	$R(7)$	1 139.917 40	−3	$R(8)$	1 144.809 60	−6
$R(9)$	1 149.550 70	−7	$R(10)$	1 154.138 70	−15	$R(11)$	1 158.571 80	−21	$R(12)$	1 162.848 40	−2
$R(13)$	1 166.966 10	−18	$R(14)$	1 170.922 40	−145	$R(15)$	1 174.719 30	−13	$R(16)$	1 178.351 30	−7
$R(17)$	1 181.817 90	−18	$R(18)$	1 185.117 80	−19	$R(19)$	1 188.249 50	−12	$R(20)$	1 191.211 30	−21
$R(21)$	1 194.002 10	−17	$R(22)$	1 196.620 30	−27	$R(23)$	1 199.065 00	−11	$R(24)$	1 201.334 70	4
$R(25)$	1 203.428 00	−5	$R(26)$	1 205.344 10	−5	$R(27)$	1 207.082 00	11	$R(28)$	1 208.640 10	−17
$R(29)$	1 210.018 30	−3	$R(30)$	1 211.215 20	3	$R(31)$	1 212.229 00	−95	$R(32)$	1 213.060 80	−108
$R(33)$	1 213.710 50	27	$R(34)$	1 214.175 00	68	$R(35)$	1 214.454 20	66	$R(36)$	1 214.547 30	−2
$R(42)$	1 211.191 30	53	$R(43)$	1 209.975 00	−8						

(5, 4) Band

Line	Observed	Δ	Line	Observed	Δ	Line	Observed	Δ	Line	Observed	Δ
			$P(27)$	867.150 60	−100	$P(25)$	884.223 95	24	$P(24)$	892.657 18	−4
$P(23)$	901.018 59	−45	$P(22)$	909.307 03	36	$P(21)$	917.518 05	46	$P(20)$	925.649 24	−6
$P(19)$	933.698 72	−57	$P(18)$	941.665 89	85	$P(17)$	949.543 89	−14	$P(16)$	957.333 42	−34
$P(15)$	965.031 78	6	$P(14)$	972.634 88	−52	$P(13)$	980.142 27	−3	$P(12)$	987.550 03	9
$P(11)$	994.856 12	29	$P(10)$	1 002.058 10	59	$P(9)$	1 009.152 70	19	$P(8)$	1 016.138 50	10
$P(7)$	1 023.012 90	17	$P(6)$	1 029.773 40	29	$P(5)$	1 036.427 30	1016	$P(4)$	1 042.942 40	−3
$P(3)$	1 049.347 20	55	$P(2)$	1 055.627 10	−36	$P(1)$	1 061.784 70	215	$R(0)$	1 073.700 80	−569
$R(1)$	1 079.470 90	3	$R(2)$	1 085.100 40	−19	$R(3)$	1 090.593 60	12	$R(4)$	1 095.947 30	−12
$R(5)$	1 101.160 20	−11	$R(6)$	1 106.230 20	10	$R(7)$	1 111.154 90	13	$R(8)$	1 115.932 30	−2
$R(9)$	1 120.560 70	−14	$R(10)$	1 125.038 40	0	$R(11)$	1 129.363 00	−16	$R(12)$	1 133.533 30	0
$R(13)$	1 137.546 80	−24	$R(14)$	1 141.402 60	−7	$R(15)$	1 145.098 50	−1	$R(16)$	1 148.632 80	−12
$R(17)$	1 152.004 40	8	$R(18)$	1 155.210 90	−29	$R(19)$	1 158.251 90	−13	$R(20)$	1 161.125 30	−11
$R(21)$	1 163.830 00	4	$R(22)$	1 166.364 00	−34	$R(23)$	1 168.727 30	2	$R(24)$	1 170.922 40	485
$R(25)$	1 172.933 80	−19	$R(26)$	1 174.775 50	2	$R(27)$	1 176.440 40	−55	$R(28)$	1 177.929 40	0
$R(29)$	1 179.239 50	−37	$R(30)$	1 180.371 50	4	$R(31)$	1 181.323 20	−12	$R(32)$	1 182.094 90	24
$R(33)$	1 182.693 10	836	$R(34)$	1 183.092 70	−17	$R(35)$	1 183.318 60	19	$R(36)$	1 183.360 10	−69
$R(37)$	1 183.218 80	−67	$R(38)$	1 182.894 20	23	$R(39)$	1 182.384 50	65	$R(40)$	1 181.687 80	−93
$R(41)$	1 180.808 00	−28	$R(43)$	1 178.489 50	−73						

(6, 5) Band

Line	Observed	Δ	Line	Observed	Δ	Line	Observed	Δ	Line	Observed	Δ
			$P(21)$	893.270 24	−20	$P(20)$	901.242 51	−101	$P(19)$	909.136 75	80
$P(18)$	916.945 93	67	$P(17)$	924.670 63	166	$P(13)$	954.657 64	−78	$P(10)$	976.131 00	3
$P(7)$	996.657 87	133	$P(5)$	1 009.782 20	2	$P(4)$	1 016.171 30	81	$P(3)$	1 022.439 50	14
$R(1)$	1 051.912 30	−19	$R(2)$	1 057.417 60	28	$R(3)$	1 062.786 90	−26	$R(4)$	1 068.020 30	38
$R(5)$	1 073.113 90	37	$R(6)$	1 078.065 90	−5	$R(7)$	1 082.875 00	−20	$R(8)$	1 087.539 70	40
$R(9)$	1 092.056 50	16	$R(10)$	1 096.424 50	5	$R(11)$	1 100.642 00	22	$R(12)$	1 104.706 60	5
$R(13)$	1 108.617 00	1	$R(14)$	1 112.371 40	0	$R(15)$	1 115.968 20	7	$R(16)$	1 119.405 80	25
$R(17)$	1 122.681 90	−20	$R(18)$	1 125.796 30	4	$R(19)$	1 128.746 50	−5	$R(20)$	1 131.531 80	24
$R(21)$	1 134.149 80	−11	$R(22)$	1 136.599 90	−38	$R(23)$	1 138.881 40	0	$R(24)$	1 140.992 10	5
$R(25)$	1 142.931 20	13	$R(26)$	1 144.697 30	−3	$R(27)$	1 146.289 30	−47	$R(28)$	1 147.707 60	23
$R(29)$	1 148.949 70	51	$R(30)$	1 150.014 90	61	$R(31)$	1 150.902 20	37	$R(32)$	1 151.610 20	−80
$R(33)$	1 152.140 10	−94	$R(35)$	1 152.657 90	−304	$R(37)$	1 152.490 40	3395	$R(38)$	1 152.082 40	122
$R(39)$	1 151.523 60	35									

(7, 6) Band

Line	Observed	Δ	Line	Observed	Δ	Line	Observed	Δ	Line	Observed	Δ
$R(4)$	1 040.544 50	−102	$R(5)$	1 045.522 60	148	$R(6)$	1 050.356 80	−57	$R(7)$	1 055.051 90	−40
$R(8)$	1 059.604 60	64	$R(9)$	1 064.011 10	64	$R(10)$	1 068.269 30	−65	$R(11)$	1 072.380 90	31

TABLE I. (Continued.)

Line	Observed	Δ	Line	Observed	Δ	Line	Observed	Δ	Line	Observed	Δ
R(12)	1 076.340 40	−22	R(13)	1 080.147 90	−40	R(14)	1 083.802 00	6	R(15)	1 087.300 10	22
R(16)	1 090.640 40	−13	R(17)	1 093.822 20	−13	R(18)	1 096.843 60	−17	R(19)	1 099.703 70	32
R(20)	1 102.400 00	25	R(22)	1 107.297 50	16	R(23)	1 109.495 90	−7	R(24)	1 111.527 00	82
R(25)	1 113.387 30	50	R(26)	1 115.077 00	31	R(27)	1 116.594 90	10	R(28)	1 117.939 30	−79
R(29)	1 119.111 80	21	R(31)	1 120.929 00	−54	R(32)	1 121.574 40	11			

while the mass-reduced Dunham U_{ij} constants listed in Table III under the column heading "unconstrained fit" were obtained from a combined fit of isotopomer data to[42,43]

$$E(v,J) = \sum_{i,j} \mu^{-(i+2j)/2} U_{ij} \left(1 + \frac{m_e}{M_A} \Delta_{ij}^A + \frac{m_e}{M_B} \Delta_{ij}^B \right)$$
$$\times \left(v + \frac{1}{2} \right)^i [J(J+1)]^j, \qquad (2)$$

where m_e is electron mass, M_A and M_B are atomic masses for centers A and B, and the Δ_{ij}'s are Born–Oppenheimer breakdown constants. Since only one naturally occurring isotope of aluminum exists, all isotopic information on Born–Oppenheimer breakdown is confined to the hydrogen center, thus only Δ_{ij}'s for the hydrogen center are determined from a least-squares fit of the data. Finally, the set of U_{ij}'s appearing in the Table III column labeled "constrained" were obtained from a fit where the U_{ij}'s for $j < 2$ were treated as adjustable parameters and all remaining U's were fixed to values determined from the constrained U relations of the Dunham model.[44,45] The standard deviations of the "unconstrained" and "constrained" fits were 0.638 and 0.682, respectively.

TABLE II. Dunham Y_{ij} constants for ^{27}AlH and ^{27}AlD in cm^{-1}.

	^{27}AlH	^{27}AlD
Y_{10}	1 682.374 74(31)	1 211.774 02(15)
Y_{20}	−29.050 978(287)	−15.064 765(114)
Y_{30}	0.247 615(115)	0.092 442 5(369)
$10^3 Y_{40}$	−1.408 1(210)	−0.381 99(525)
$10^4 Y_{50}$	−1.304 7(142)	−0.251 01(272)
Y_{01}	6.393 784 18(169)	3.318 392 93(80)
Y_{11}	−0.187 052 66(148)	−0.069 877 296(436)
$10^3 Y_{21}$	1.818 302(980)	0.489 018(275)
$10^7 Y_{31}$	−3.08(249)	−1.990(818)
$10^6 Y_{41}$	−1.888 4(216)	−0.241 6(107)
$10^{10} Y_{51}$		−8.37(519)
$10^4 Y_{02}$	−3.685 327 1(597)	−0.994 169 2(132)
$10^6 Y_{12}$	6.418 77(318)	1.244 146(439)
$10^8 Y_{22}$	1.402(175)	0.267 0(117)
$10^9 Y_{32}$	−6.324(396)	−0.750 9(238)
$10^{10} Y_{42}$	−2.909(305)	−0.185 1(177)
$10^8 Y_{03}$	1.503 582(621)	0.211 980 8(977)
$10^{10} Y_{13}$	−1.286 2(278)	−0.120 02(202)
$10^{11} Y_{23}$	−1.564 3(683)	−0.141 44(207)
$10^{13} Y_{33}$	−7.59(102)	
$10^{13} Y_{04}$	−7.200 1(538)	−0.540 86(370)

TABLE III. (a) Mass-reduced Dunham constants in cm^{-1}. See text for explanation of unconstrained and constrained fits. (b) Born–Oppenheimer breakdown constants for hydrogen center.

	Unconstrained	Constrained
(a)		
U_{10}	1 659.612 53(19)	1 659.613 24(13)
U_{20}	−28.244 454(190)	−28.245 378(117)
U_{30}	0.237 166 2(807)	0.237 602 2(469)
$10^3 U_{40}$	−1.336 7(152)	−1.428 39(818)
$10^4 U_{50}$	−1.209 6(104)	−1.140 23(519)
U_{01}	6.226 876 30(312)	6.226 886 81(117)
U_{11}	−0.179 460 52(120)	−0.179 463 559(329)
$10^3 U_{21}$	1.718 576(974)	1.721 117(193)
$10^6 U_{31}$	−0.872(359)	−1.563 9(615)
$10^6 U_{41}$	−1.647 3(600)	−1.500 71(959)
$10^8 U_{51}$	−0.378(379)	−1.734 5(472)
$10^4 U_{02}$	−3.506 006(101)	−3.506 381 16
$10^6 U_{12}$	6.009 30(229)	6.021 884 72
$10^9 U_{22}$	12.36(112)	5.386 837 55
$10^9 U_{32}$	−5.584(257)	−5.199 051 65
$10^{10} U_{42}$	−2.729(199)	−2.419 995 72
$10^8 U_{03}$	1.413 93(139)	1.421 142 12
$10^{10} U_{13}$	−1.127 8(157)	−1.257 135 66
$10^{12} U_{23}$	−14.209(471)	−5.074 912 52
$10^{12} U_{33}$	−0.632 9(692)	−1.321 486 20
$10^{15} U_{43}$		5.710 413 29
$10^{13} U_{04}$	−6.875 9(641)	−7.798 061 27
$10^{16} U_{14}$		−5.417 936 38
$10^{15} U_{24}$		−1.961 808 03
$10^{17} U_{34}$		6.517 990 20
$10^{17} U_{05}$		5.019 229 90
$10^{19} U_{15}$		3.944 324 47
$10^{19} U_{25}$		−1.190 762 41
$10^{20} U_{35}$		−2.470 022 15
$10^{21} U_{06}$		−3.631 957 40
$10^{22} U_{16}$		−3.368 378 43
$10^{23} U_{26}$		1.936 313 89
$10^{25} U_{07}$		2.750 145 27
$10^{26} U_{17}$		2.849 944 21
$10^{27} U_{27}$		−7.710 794 32
$10^{29} U_{08}$		−2.622 289 02
$10^{30} U_{18}$		−2.992 713 00
$10^{33} U_{09}$		2.269 982 74
$10^{36} U_{19}$		−5.873 323 38
$10^{37} U_{010}$		−2.160 908 13
$10^{41} U_{011}$		1.777 605 42
(b)		
Δ_{10}^H	−1.499 060(102)	−1.498 956(104)
Δ_{20}^H	−1.317 49(113)	−1.317 87(115)
Δ_{01}^H	−4.451 31(113)	−4.452 768(540)
Δ_{11}^H	−3.438 16(473)	−3.434 04(316)
Δ_{21}^H	−0.707 4(665)	−0.792 9(597)
Δ_{02}^H	−14.447 5(658)	−14.430 9(193)
Δ_{12}^H	−11.970(293)	−12.012 2(995)
Δ_{03}^H	−46.36(219)	−42.308(581)
Δ_{04}^H	−107.9(151)	−62.66(340)

An effective Born–Oppenheimer potential was determined from a least-squares fit of the combined AlH and AlD data to the eigenvalues of the radial Schrödinger equation

$$\left| \frac{\hbar^2}{2\mu} \nabla^2 - U^{\mathrm{eff}}(R) + E(v,J) - \frac{\hbar^2}{2\mu}[1+q(R)]J(J+1)/R^2 \right|$$

$$\times \psi(r;v,J) = 0, \tag{3}$$

where the effective internuclear potential for vibrational motion is given by

$$U^{\mathrm{eff}}(R) = U^{\mathrm{BO}}(R) + U_A(R)/M_A + U_B(R)/M_B \tag{4}$$

and the form of the Born–Oppenheimer potential is chosen to be

$$U^{\mathrm{BO}}(R) = D_e\{1 - \exp[-\beta(R)]\}^2/\{1 - \exp[-\beta(\infty)]\}^2, \tag{5}$$

where

$$\beta(R) = z \sum_{i=0} \beta_i z^i, \tag{6}$$

$$\beta(\infty) = \sum_{i=0} \beta_i, \tag{7}$$

and

$$z = (R - R_e)/(R + R_e). \tag{8}$$

The remaining terms in Eq. (4) are corrections for atomic centers A and B which take into account Born–Oppenheimer breakdown and homogeneous nonadiabatic mixing from distant Σ electronic states and are represented by the power series expansions

$$U_A(R) = \sum_{i=1} u_i^A (R - R_e)^i \tag{9}$$

and

$$U_B(R) = \sum_{i=1} u_i^B (R - R_e)^i. \tag{10}$$

Similarly, J-dependent Born–Oppenheimer breakdown and heterogeneous nonadiabatic mixing from distant Π states are accounted for by the $q(R)$ term in Eq. (4) where

$$q(R) = M_A^{-1} \sum_{i=0} q_i^A (R - R_e)^i + M_B^{-1} \sum_{i=0} q_i^B (R - R_e)^i. \tag{11}$$

Our fitting procedure is similar to the method reported by Coxon and Hajigeorgiou[46,47] and is described in greater detail elsewhere.[45,48]

Results from the potential model fit are displayed in Table IV. Potential parameters that were statistically determined are listed along with their uncertainties quoted to one standard deviation. The standard deviation of the fit was 0.953. The dissociation energy and the atomic masses in Table IV were obtained from Refs. 49 and 50, respectively.

A plot of the Born–Oppenheimer potential function [Eq. (5)] is displayed in Fig. 5. In addition the CASSCF potential, reported by Matos et al.,[15] has also been in-

TABLE IV. Internuclear potential parameters.

Parameter	Value	Uncertainty
$10^{-4}D_e$ (cm^{-1})	2.460 000 000 000 000 000	
R_e (Å)	1.645 362 224 046 089	2.13×10^{-7}
β_0	4.240 357 942 342 511	9.63×10^{-7}
β_1	3.562 083 595 686 275	1.82×10^{-5}
β_2	5.749 940 272 769 324	2.20×10^{-4}
$10^{-1}\beta_3$	1.145 462 084 579 327	2.38×10^{-4}
$10^{-1}\beta_4$	2.382 781 031 109 177	2.39×10^{-3}
$10^{-1}\beta_5$	6.109 165 969 369 654	1.44×10^{-2}
$10^{-1}\beta_6$	4.444 140 528 758 436	9.49×10^{-2}
$10^{-2}\beta_7$	$-3.043 307 109 330 400$	4.16×10^{-2}
$10^{-3}\beta_8$	2.055 792 529 818 816	8.95×10^{-3}
$10^{-2}\beta_9$	$-1.155 367 715 846 806$	1.21×10^{-1}
$10^{-2}u_1^H$ (cm^{-1} Å^{-1})	$-1.651 114 347 426 463$	2.56×10^{-4}
$10^{-2}u_2^H$ (cm^{-1} Å^{-2})	2.769 565 858 770 814	5.29×10^{-4}
$10^{-2}u_3^H$ (cm^{-1} Å^{-3})	$-3.216 972 749 774 876$	8.25×10^{-3}
$10^{-2}u_4^H$ (cm^{-1} Å^{-4})	3.155 411 071 812 395	2.59×10^{-2}
$10^{-2}u_5^H$ (cm^{-1} Å^{-5})	$-2.613 946 167 257 996$	3.60×10^{-2}
$10^{-2}u_6^H$ (cm^{-1} Å^{-6})	1.432 168 079 746 304	3.52×10^{-2}
$10^{-1}u_7^H$ (cm^{-1} Å^{-7})	$-1.419 335 229 284 762$	4.05×10^{-1}
$10^{-1}u_8^H$ (cm^{-1} Å^{-8})	$-2.036 051 378 935 532$	2.20×10^{-1}
$10^3 q_1^H$ (Å^{-1})	1.368 779 115 860 656	4.42×10^{-3}
$10^3 q_2^H$ (Å^{-2})	$-1.739 621 257 226 495$	3.21×10^{-2}
$10^3 q_3^H$ (Å^{-3})	1.311 049 289 402 076	4.45×10^{-2}
$10^3 q_4^H$ (Å^{-4})	$-1.121 006 077 788 522$	5.63×10^{-2}
$10^4 q_5^H$ (Å^{-5})	5.515 765 167 230 819	4.82×10^{-1}
M_A (^{27}Al)	26.981 538 6	
M_B (H)	1.007 825 035	
M_B (D)	2.014 101 779	

cluded in the plot for the purpose of comparison. Our experimental data covers the range 1.24–2.57 Å. Because the theoretical potential listed in Table III of Ref. 15 is expressed in terms of total energy, the following procedure was used to scale the theoretical potential to conform to the unitless energy scale in Fig. 5. The minimum energy at $r \approx 1.64$ Å (3.10 a.u.) was subtracted from each entry in Table III of Ref. 15 followed by scaling these values to the total energy at $r = 5.29$ Å ($r = 10.0$ a.u.) which we assume approximates the total energy at infinite internuclear separation.

As clearly demonstrated in Fig. 5, our experimentally derived Born–Oppenheimer potential is in good agreement
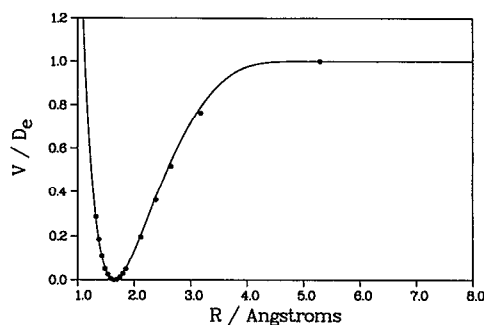

FIG. 5. Direct comparison of our AlH Born–Oppenheimer potential (smooth curve) to the theoretical CASSCF potential (discrete points) reported by Matos, Malmqvist, and Roos.

with the CASSCF theoretical potential. It is also worth mentioning that the value of the equilibrium internuclear separation predicted by the CASSCF calculation, $R_e = 1.652$ Å is in good agreement with our value, $R_e = 1.645\,362\,2(21)$ Å, obtained from the potential model fit.

IV. CONCLUSION

Detection of infrared emission with a Fourier transform spectrometer has once again proved to be a powerful technique for recording the high resolution vibrational-rotational spectra of AlH and AlD. The high quality of these data sets as exemplified by wide and continuous spectral coverage, high signal to noise spectra (≈ 150), and high precision measurements of spectral line positions (± 0.0002 cm^{-1}) has lead to significant refinement in the spectroscopic constants of the $^1\Sigma^+$ ground state. Sets of Dunham Y_{ij} constants for AlH and AlD were determined along with a set of "unconstrained" and a set of "constrained" isotopically invariant Dunham U_{ij} constants.

In addition, an effective internuclear potential energy function for the $^1\Sigma^+$ ground electronic state was derived by directly fitting the combined AlH and AlD data to the eigenvalues of the effective radial Schrödinger equation for a $^1\Sigma^+$ state. Furthermore, because transitions from our AlH and AlD data sets involve vibrational-rotational levels that span almost 50% of the potential well depth, it is quite conceivable that the effective internuclear potential energy function reported here may well prove to be instrumental in providing accurate predictions of energies (as well as other observable properties) for higher-lying vibrational-rotational levels of the ground state, perhaps even levels that lie close to the dissociation limit.

ACKNOWLEDGMENTS

[1] P. Carrick, AIAA, J. Propulsion Power (submitted).

[2] P. W. Merrill, Astrophys. J. 118, 453 (1953).

[3] G. Herbig, Pub. Astron. Soc. Pacific 68, 204 (1956).

[4] H. R. Johnson and A. J. Sauval, Astron. Astrophys. Suppl. Ser. 49, 77 (1982).

[5] P. Sotirovski, Astron. Astrophys. Suppl. 6, 85 (1972).

[6] F. Grimaldi, A. Lecourt, H. Lefebvre-Brion, and C. Moser, J. Mol. Spectrosc. 20, 341 (1966).

[7] P. Cade and W. Huo, J. Chem. Phys. 47, 649 (1967).

[8] P. Cade, R. Bader, W. Henneker, and I. Keaveny, J. Chem. Phys. 50, 5313 (1969).

[9] E. A. Laws, R. M. Stevens, and W. N. Lipscomb, J. Chem. Phys. 54, 4629 (1971).

[10] W. Meyer and P. Rosmus, J. Chem. Phys. 63, 2356 (1975).

[11] M. Pelissier and J. P. Malrieu, J. Chem. Phys. 67, 5963 (1977).

[12] N. Sabelli, M. Kantor, R. Benedek, and T. Gilbert, J. Chem. Phys. 68, 2767 (1978).

[13] F. Marinelli and A. Allouche, Theor. Chim. Acta 62, 175 (1982).

[14] G. Pacchioni, Theor. Chim. Acta 62, 461 (1983).

[15] J. M. O. Matos, Per-Åke Malmqvist, and B. O. Roos, J. Chem. Phys. 86, 5032 (1987).

[16] G. H. F. Diercksen and A. J. Sadlej, Chem. Phys. Lett. 141, 530 (1987).

[17] R. H. Tipping, A. L. Pineiro, and C. Chackerian, Astrophys. J. 323, 810 (1987).

[18] J. M. O. Matos, B. O. Roos, A. J. Sadlej, and G. H. F. Diercksen, Chem. Phys. 119, 71 (1988).

[19] C. W. Bauschlicher, Jr. and S. R. Langhoff, J. Chem. Phys. 89, 2116 (1988).

[20] G. E. Scuseria, J. Geertsen, and J. Oddershede, J. Chem. Phys. 90, 2338 (1989).

[21] G. Eriksson and E. Hulthén, Z. Phys. 34, 775 (1925).

[22] V. L. Farkas, Z. Phys. 70, 733 (1931); V. L. Farkas and S. Levy, ibid. 84, 195 (1933).

[23] V. W. Holst, Z. Phys. 86, 338 (1933); Nature 132, 297 (1933); Z. Phys. 89, 40 (1934); 90, 728 (1934); 90, 735 (1934).

[24] V. W. Holst and E. Hulthén, Z. Phys. 90, 712 (1934).

[25] V. B. Grabe and E. Hulthén, Z. Phys. 114, 470 (1939).

[26] G. Herzberg and L. G. Mundie, J. Chem. Phys. 8, 263 (1939).

[27] B. Kleman, Ark. Fys. 6, 407 (1953).

[28] P. B. Zeeman and G. J. Ritter, Can. J. Phys. 32, 555 (1954).

[29] B. Huron, Physica 41, 58 (1969).

[30] M. Rafi, M. A. Baig, and M. A. Khan, Nuovo Cimento B 43B, 271 (1978).

[31] A. Lagerqvist, L. E. Lundh, and H. Neuhaus, Phys. Scr. 1, 261 (1970).

[32] W. J. Balfour and B. Lindgren, J. Phys. B 17, L861 (1984).

[33] P. Baltayan and O. Nedelec, J. Chem. Phys. 70, 2399 (1979).

[34] Y. Zhang and M. Stuke, Chem. Phys. Lett. 149, 310 (1988); J. Phys. Chem. 93, 4503 (1989).

[35] J. Rice, L. Pasternack, and H. Nelson, Chem. Phys. Lett. 189, 43 (1992).

[36] Y. Zhu, R. Shehadeh, and E. Grant, J. Chem. Phys. 97, 883 (1992).

[37] R.-D. Urban and H. Jones, Chem. Phys. Lett. 190, 609 (1992).

[38] C. Yamada and E. Hirota, Chem. Phys. Lett. 197, 461 (1992).

[39] J. Deutsch, W. Neil, and D. Ramsay, J. Mol. Spectrosc. 125, 115 (1987).

[40] R. A. Toth, J. Opt. Soc. Am. B 8, 2236 (1991).

[41] J. L. Dunham, Phys. Rev. 41, 721 (1932).

[42] A. H. M. Ross, R. S. Eng, and H. Kildal, Opt. Commun. 12, 433 (1974).

[43] J. K. G. Watson, J. Mol. Spectrosc. 80, 411 (1980).

[44] J. Ogilvie (private communication); Comput. Phys. Commun. 30, 101 (1983).

[45] H. G. Hedderich, M. Dulick, and P. F. Bernath, J. Chem. Phys. 99, 8363 (1993).

[46] J. A. Coxon and P. G. Hajigeorgiou, Can. J. Phys. 70, 40 (1992).

[47] J. A. Coxon and P. G. Hajigeorgiou, Chem. Phys. 167, 327 (1992).

[48] M. Dulick and P. F. Bernath (in preparation).

[49] K. P. Huber and G. Herzberg, Constants of Diatomic Molecules (Van Nostrand-Reinhold, New York, 1979).

[50] I. Mills, Quantities, Units and Symbols in Physical Chemistry (Blackwell, Oxford, UK, 1989).